High-mobility (>100 $cm^2V^{-1}s^{-1}$) In_2O_3:H Thin-film Transistors by Solid-phase Crystallization

Yusaku Magari[1], **Wenchang Yeh**[2], **and Mamoru Furuta**[3]

magari.yusaku@es.hokudai.ac.jp
[1] Research Institute for Electronic Science, Hokkaido University, Sapporo 001-0020, Japan
[2] Graduate School of Natural Science and Technology, Shimane University, Matsue, 690-8504, Japan
[3] School of Environmental Science and Engineering, Kochi University of Technology, Kami 782-8502, Japan
Keywords: Polycrystalline oxide semiconductors, In_2O_3:H, solid-phase crystallization, thin-film transistors, high mobility

ABSTRACT

We propose a simple process to obtain high-performance thin-film transistors (TFTs), namely hydrogenated polycrystalline In_2O_3 (In_2O_3:H) TFTs grown via the low-temperature solid-phase crystallization (SPC) process. In_2O_3:H TFTs fabricated at 300 °C exhibit superior switching properties with field-effect mobility of 139.2 $cm^2V^{-1}s^{-1}$, a subthreshold swing of 0.19 $Vdec^{-1}$, and a threshold voltage of 0.2 V.

1 Introduction

Amorphous oxide semiconductors (AOSs) have been extensively studied as active channel layers of thin-film transistors (TFTs) for backplane of LCDs and OLED displays.[1-4] This is because AOSs represented by amorphous In–Ga–Zn–O (a-IGZO) has properties that are superior to hydrogenated amorphous Si (a-Si:H), such as a large field-effect mobility (μ_{FE}) of over 10 $cm^2V^{-1}s^{-1}$, an extremely low leakage current, a low processing temperature (<350 °C), and large-area scalability.[1-4] Although the μ_{FE} value of a-IGZO TFTs is more than ten times higher than that of a-Si:H TFTs (<1 cm^2 V^{-1} s^{-1}), the further improvement of μ_{FE} values is required to expand their range of applications as alternatives to poly-Si TFTs (~100 cm^2 V^{-1} s^{-1}).

The optimization of AOS composition is one approach for improving μ_{FE}; for example, an increase in the In ratio due the considerable spatial spread of the In 5*s* orbital with a large overlap can provide a facile electron transport path with a low electron effective mass.[5-7] Although the various AOS compositions have been proposed, the μ_{FE} value remains insufficiently high to compete with that of poly-Si TFTs.

In contrast, the crystallization of OSs is an another approach for improving μ_{FE}, because the subgap density of states originating from structural disorder and defects can be suppressed via lattice ordering. Although polycrystalline OSs, including In_2O_3, ZnO, and SnO_2, have been investigated as channel materials in early oxide-based TFTs, they can easily create oxygen vacancies, leading to degenerate semiconductors.[8-10] In addition, μ_{FE} degradation due to grain boundary scattering is a serious issue for polycrystalline OSs as well as poly-Si.[11] Polycrystalline In_2O_3 films have been investigated for use as the transparent conductive oxide (TCO) in solar cells. Koida et al. reported a degenerate hydrogen-doped polycrystalline In_2O_3 film with high electron mobility (100–130 $cm^2V^{-1}s^{-1}$) produced by solid-phase crystallization (SPC).[12]

This study proposes a simple material and a simple process to obtain high-performance TFTs, namely hydrogenated polycrystalline In_2O_3 (In_2O_3:H) TFTs grown via the low-temperature SPC process.[13] We believe these SPC-grown In_2O_3:H TFTs have a great potential for use in future electronics applications.

2 Experimental

In_2O_3:H TFTs were fabricated on a heavily doped *p*-type Si substrate with a 100-nm-thick thermally grown SiO_2. The doped *p*-type Si substrate and the SiO_2 were used as the gate electrode and the gate insulator. The 30-nm-thick In_2O_3 and In_2O_3:H channels were deposited via pulsed direct-current (DC) magnetron sputtering without substrate heating from a ceramic In_2O_3 target using a mixture of Ar, O_2, and H_2 gases. The O_2 and H_2 gas flow ratios are $R[O_2] = O_2/(Ar+O_2+H_2)$ and $R[H_2] = H_2/(Ar+O_2+H_2)$, respectively. For the Ar+O_2-sputtered In_2O_3 film, $R[O_2]$ was set to 1% without H_2 introduction ($R[H_2]$ = 0%). For the Ar+O_2+H_2-sputtered In_2O_3 film (In_2O_3:H), $R[O_2]$ and $R[H_2]$ were 1% and 5%, respectively. The deposition pressure and DC power were maintained at 0.6 Pa and 50 W, respectively. The base pressure before gas introduction was below 6×10^{-5} Pa. The In_2O_3 and In_2O_3:H films were then annealed in ambient air at 300 °C for 1 h. After annealing, a 100-nm-thick SiO_2 film was deposited via reactive sputtering without substrate heating. This film served as a passive layer. Subsequently, Al source/drain electrodes were deposited via sputtering. Finally, In_2O_3 and In_2O_3:H TFTs were annealed at 250 °C in ambient air for 1 h. The In_2O_3, SiO_2, and Al films were deposited through a shadow mask. Both the channel length and the width were 300 µm.

3 Results and discussion

3.1 Structural properties of the In_2O_3 and In_2O_3:H films.

Figure 1 depicts the Electron backscattering diffraction (EBSD) images of the (a) In_2O_3 (R[H_2] = 0%) and (b) In_2O_3:H (R[H_2] = 5%) films before and after annealing at 250 °C. For the as-deposited In_2O_3 film, a randomly oriented small grain structure embedded in the amorphous matrix can be observed. The grain structure disappeared by introducing hydrogen during sputtering. In contrast, a huge grain structure appeared for In_2O_3:H film after annealing at 250 °C, indicating SPC occurrence. The EBSD results show that the nuclei density in the as-deposited film was suppressed by introducing hydrogen during sputtering. Because of the reduction in the nuclei density in the initial In_2O_3:H film, the grain size of the In_2O_3:H film could be enlarged through SPC. Thus, the controlling the crystallinity and nuclei density in the as-deposited film are key factors to achieve high-quality In_2O_3:H films.

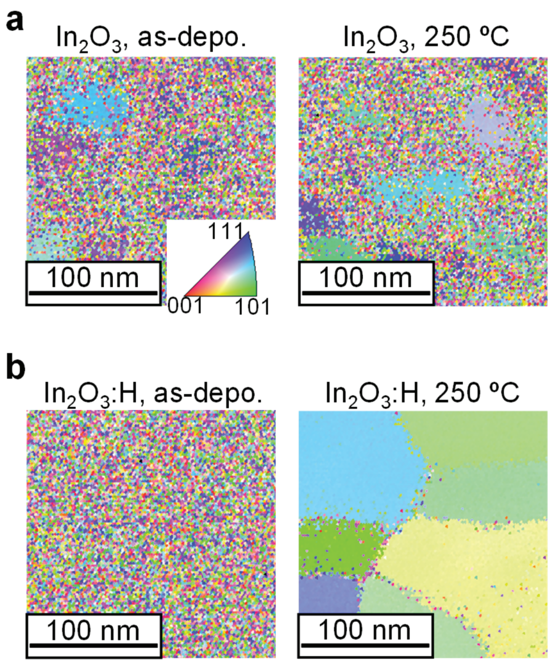

Fig. 1. Structural properties of the In_2O_3 and In_2O_3:H films. EBSD images of the (a) In_2O_3 (R[H_2] = 0%) and (b) In_2O_3:H (R[H_2] = 5%) films before and after annealing at 250 °C.

Figure 2 shows the Hard X-ray photoelectron spectroscopy (HAXPES) spectra around the bandgap energy (E_g) region obtained from the In_2O_3 and In_2O_3:H films before and after annealing at 300 °C in ambient air. For the as-deposited films, the near-valence band maximum (near-VBM) and the near-conduction band minimum (near-CBM) states significantly increased by introducing hydrogen. In contrast, both the near-VBM and near-CBM states in the In_2O_3:H film decreased after annealing at 300 °C, resulting that the density of near-CBM states in the In_2O_3:H was lower than that in the In_2O_3 after annealing at 300 °C. The reduction of the near-CBM states is expected to strongly affect the carrier transport properties of the film.[14] HAXPES analysis revealed that indicating that the SPC process is effective for reducing the number of subgap defects.

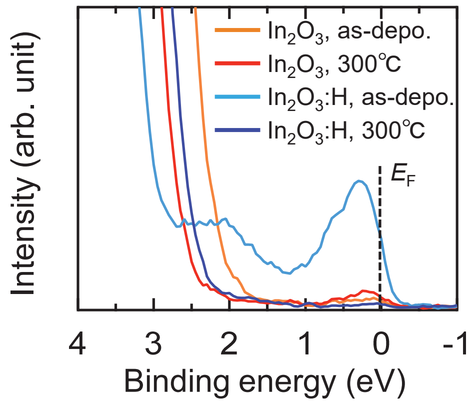

Fig. 2. Subgap states in the In_2O_3 and In_2O_3:H films. HAXPES spectra around E_g region obtained from the In_2O_3 and In_2O_3:H films before and after annealing at 300 °C in ambient air.

3.2 Electrical properties of the In_2O_3 and In_2O_3:H films.

Figures 3a and 3b show the Hall mobility (μ_{Hall}) and carrier concentration (N_e) of the 50-nm-thick In_2O_3 and In_2O_3:H films as a function of the annealing temperature. In_2O_3 without hydrogen introduction exhibited an almost constant μ_{Hall} value over the entire range of investigated annealing temperature values, as shown in Fig. 3a. In contrast, upon annealing at 200 °C, the μ_{Hall} of In_2O_3:H film increased to 104.0 $cm^2V^{-1}s^{-1}$, indicating that the SPC started at an annealing temperature value between 150 °C and 200 °C. The increased μ_{Hall} is attributable to the increased grain size, as shown in Fig. 1b. The obtained μ_{Hall} value is five times higher than that of the In_2O_3 film.

Regarding the N_e of the films, for the as-deposited films, N_e increased from 7.1 × 10^{19} to 5.7 × 10^{20} cm^{-3} by introducing hydrogen, as shown in Fig. 3b. Since hydrogen acts as a shallow donor in In_2O_3,[15] the increase in the N_e of the as-deposited In_2O_3:H film is attributable to hydrogen doping effects. The In_2O_3 film deposited without hydrogen introduction exhibited an almost constant N_e value over the whole range of investigated annealing temperature values. On the other hand, the N_e of the In_2O_3:H film rapidly decreased for annealing temperature higher than 200 °C where SPC occurs. As a result, an appropriate N_e value of 2.0 × 10^{17} cm^{-3} for TFT fabrication was obtained at annealing temperature of 300 °C for the In_2O_3:H film. This N_e value is over two orders of magnitude lower than that of the

In_2O_3 film deposited without hydrogen introduction (3.0 × 10^{19} cm^{-3}). Although adding H_2 induced the formation of free carriers in the as-deposited films, the N_e of the films could be reduced via the relatively low-temperature SPC process and became comparable to that of single-crystalline epitaxial In_2O_3 films deposited at 650 °C (~1 × 10^{17} cm^{-3}).[16]

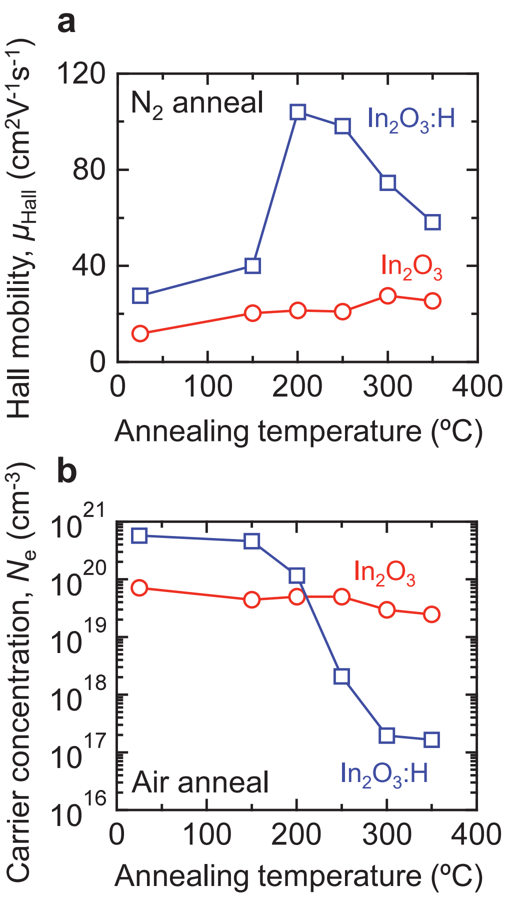

Fig. 3. Electrical properties of the In_2O_3 and In_2O_3:H films. (a) μ_{Hall} and (b) N_e of In_2O_3 and In_2O_3:H films as a function of the annealing temperature.

3.3 In_2O_3 and In_2O_3:H TFT characteristics.

Figure 4 shows typical transfer characteristics of the TFTs with In_2O_3 and In_2O_3:H channels. All TFTs were fabricated using annealing in ambient air at 300 °C. The In_2O_3 TFT without H_2 introduction did not exhibit any switching (conductive behavior) because the In_2O_3 film was still in a degenerated state (Fig. 3b). By contrast, the In_2O_3:H TFT exhibited a switching with an extremely high μ_{FE} of 139.2 $cm^2V^{-1}s^{-1}$, a subthreshold swing (*SS*) of 0.19 $Vdec^{-1}$, a threshold voltage (V_{th}) of 0.2 V. The obtained μ_{FE} value is comparable to the μ_{Hall} of epitaxial single-crystal In_2O_3 films (~160 $cm^2V^{-1}s^{-1}$).[17] The resulting transfer performance of the SPC-prepared In_2O_3:H TFT was superior to that of previously reported oxide-based TFTs.[18]

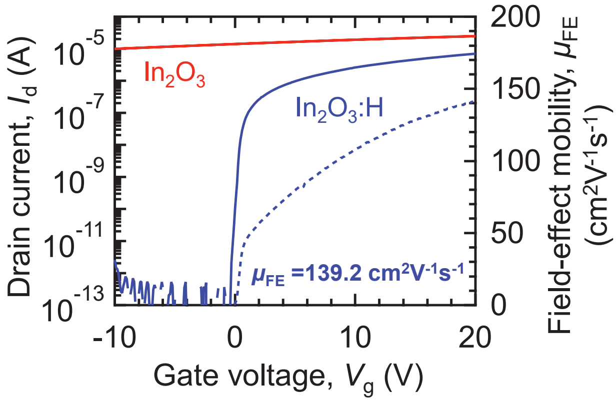

Fig. 4. In_2O_3 and In_2O_3:H TFT characteristics. Typical transfer characteristics of the TFTs with In_2O_3 and In_2O_3:H channels annealed at 300 °C in ambient air.

Figure 5 shows the bright-field high-resolution transmission electron microscopy (HRTEM) image and selective area electron diffraction (SAED) pattern obtained from the SPC-prepared In_2O_3:H TFT. A clear lattice image was observed over the entire thickness of the In_2O_3:H channel. Moreover, there was a single crystal-like diffraction pattern in the SAED pattern, even in the thin layers, roughly at a distance of 5 nm from the SiO_2 gate insulator.

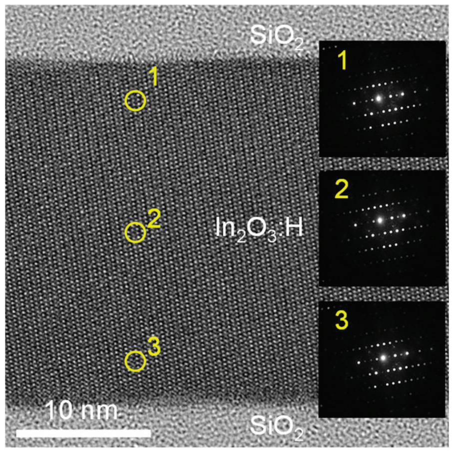

Fig. 5. Cross-sectional view of the SPC-prepared In_2O_3:H TFT. HRTEM image and corresponding SAED pattern of the active layer of the TFT with In_2O_3:H channel.

4 Conclusions

In this study, we demonstrate the high-performance polycrystalline In_2O_3:H TFTs using a low-temperature SPC process. The In_2O_3:H TFT exhibits an extremely high μ_{FE} of 139.2 $cm^2V^{-1}s^{-1}$, an appropriate V_{th} of 0.2 V, and a small *SS* of 0.19 $Vdec^{-1}$. The hydrogen introduced during sputter deposition plays an important role in enlarging the grain size and decreasing the subgap defects in SPC-prepared In_2O_3:H. The proposed method does not require any additional expensive equipment and/or change in the conventional oxide TFT fabrication process. We believe that these SPC-grown In_2O_3:H TFTs are promising candidates for use in future electronics applications.

References

[1] K. Nomura, H. Ohta, A. Takagi, T. Kamiya, M. Hirano, and H. Hosono, "Room-temperature fabrication of transparent flexible thin-film transistors using amorphous oxide semiconductors," *Nature,* vol. 432, no. 7016, pp. 488-92 (2004).

[2] H. Hosono, "How we made the IGZO transistor," *Nat Electron,* vol. 1, no. 7, pp. 428-428 (2018).

[3] H. Hosono and H. Kumomi,. *Amorphous oxide semiconductors: IGZO and related materials for display and memory*. Eds. Wiley: Hoboken, NJ (2022).

[4] T. Kamiya and H. Hosono, "Material characteristics and applications of transparent amorphous oxide semiconductors," *Npg Asia Materials,* vol. 2, no. 1, pp. 15-22 (2010).

[5] K. Nomura, H. Ohta, K. Ueda, T. Kamiya, M. Hirano, and H. Hosono, "Thin-film transistor fabricated in single-crystalline transparent oxide semiconductor," *Science,* vol. 300, no. 5623, pp. 1269-1272 (2003).

[6] Y. S. Shiah *et al.*, "Mobility-stability trade-off in oxide thin-film transistors," *Nat Electron,* vol. 4, no. 11, pp. 800-807 (2021).

[7] D. Koretomo, S. Hamada, M. Mori, Y. Magari, and M. Furuta, "Marked improvement in reliability of 150 degrees C processed IGZO thin-film transistors by applying hydrogenated IGZO as a channel material," *Applied Physics Express,* vol. 13, no. 7 (2020).

[8] Dhananjay and C. W. Chu, "Realization of In2O3 thin film transistors through reactive evaporation process," *Applied Physics Letters,* vol. 91, no. 13 (2007).

[9] T. Hirao *et al.*, "Novel top-gate zinc oxide thin-film transistors (ZnO TFTs) for AMLCDs," *Journal of the Society for Information Display,* vol. 15, no. 1, pp. 17-22 (2007).

[10] R. E. Presley, C. L. Munsee, C. H. Park, D. Hong, J. F. Wager, and D. A. Keszler, "Tin oxide transparent thin-film transistors," *J Phys D Appl Phys,* vol. 37, no. 20, pp. 2810-2813 (2004).

[11] S. Higashi, K. Ozaki, K. Sakamoto, Y. Kano, and T. Sameshima, "Electrical properties of excimer-laser-crystallized lightly doped polycrystalline silicon films," *Jpn J Appl Phys 2,* vol. 38, no. 8a, pp. L857-L860 (1999).

[12] T. Koida, H. Fujiwara, and M. Kondo, "Hydrogen-doped In2O3 as High-mobility Transparent Conductive Oxide," *Japanese Journal of Applied Physics,* vol. 46, no. No. 28, pp. L685-L687 (2007).

[13] Y. Magari, T. Kataoka, W. Yeh, and M. Furuta, "High-mobility hydrogenated polycrystalline In2O3 (In2O3:H) thin-film transistors," *Nat Commun,* vol. 13, no. 1, p. 1078 (2022).

[14] Y. Magari *et al.*, "Record-High-Performance Hydrogenated In-Ga-Zn-O Flexible Schottky Diodes," *ACS Appl Mater Interfaces,* vol. 12, no. 42, pp. 47739-47746 (2020).

[15] P. D. C. King *et al.*, "Shallow donor state of hydrogen in In2O3 and SnO2: Implications for conductivity in transparent conducting oxides," *Physical Review B,* vol. 80, no. 8 (2009).

[16] N. Preissler, O. Bierwagen, A. T. Ramu, and J. S. Speck, "Electrical transport, electrothermal transport, and effective electron mass in single-crystalline In2O3 films," *Physical Review B,* vol. 88, no. 8 (2013).

[17] R. L. Weiher, "Electrical Properties of Single Crystals of Indium Oxide," *Journal of Applied Physics,* vol. 33, no. 9, pp. 2834-& (1962).

[18] S. Y. Lee, "Comprehensive Review on Amorphous Oxide Semiconductor Thin Film Transistor," *Transactions on Electrical and Electronic Materials,* vol. 21, no. 3, pp. 235-248 (2020).